The added value of convection permitting simulations of extreme precipitation events over the eastern Mediterranean

Zittis G.[1*], Bruggeman A.[1], Camera C.[1], Hadjinicolaou P.[1], Lelieveld J.[1,2]

1 Energy Environment and Water Research Center, The Cyprus Institute, Nicosia, Cyprus

2 Dept. of Atmospheric Chemistry, Max Plank Institute for Chemistry, Mainz, Germany

*corresponding author e-mail: g.zittis@cyi.ac.cy

Highlights

- WRF simulations captured rainfall reasonably well for three of the five extreme events.
- The BMJ and GF convection and Ferrier, WDM6 and WSM6 microphysics parameterizations are found to outperform.
- Convection-permitting simulations add a value, especially over regions of high-elevation
- Significant discrepancies between three, gridded precipitation datasets are reported.

Abstract. Climate change is expected to substantially influence precipitation amounts and distribution. To improve simulations of extreme rainfall events, we analyzed the performance of different convection and microphysics parameterizations of the WRF (Weather Research and Forecasting) model at very high horizontal resolutions (12, 4 and 1 km). Our study focuses on the eastern Mediterranean climate change hot-spot. Five extreme rainfall events over Cyprus were identified from observations and were dynamically downscaled from the ERA-Interim (EI) dataset with WRF. We apply an objective ranking scheme, using a 1-km gridded observational dataset over Cyprus and six different performance metrics, to investigate the skill of the WRF configurations. We evaluate the rainfall timing and amounts for the different resolutions, and discuss the observational uncertainty over the particular extreme events by comparing three gridded precipitation datasets (E-OBS, APHRODITE and CHIRPS). Simulations with WRF capture rainfall over the eastern Mediterranean reasonably well for three of the five selected extreme events. For these three cases, the WRF simulations improve the ERA-Interim data, which strongly underestimate the rainfall extremes over Cyprus. The best model performance is obtained for the January 1989 event, simulated with an average bias of 4% and a modified Nash-Sutcliff of 0.72 for the 5-member ensemble of the 1-km simulations. We find overall added value for convection-permitting simulations, especially over regions of high-elevation. Interestingly, for some cases the intermediate 4-km nest was found to outperform the 1-km simulations for low-elevation coastal parts of Cyprus. Finally, we find significant and inconsistent discrepancies between the three, state of the art, gridded precipitation datasets for the tested events, highlighting the observational uncertainty in the region.

Key words: Regional climate modeling, Weather Research and Forecasting model, extreme precipitation, convection-permitting simulations, hydro-climatology, eastern Mediterranean, Cyprus

Version: Accepted manuscript version of the paper published in Atmospheric Research (https://doi.org/10.1016/j.atmosres.2017.03.002)

1. Introduction

While global climate projections for temperature, which indicate a general warming, appear to be reasonably robust, this is not the case for precipitation changes (Collins et al., 2013; Lelieveld et al., 2016). Model results and measurements can vary considerably and depend strongly on the region of interest. Discrepancies, even in the sign and the amount of precipitation changes, can occur among climate models. Accordingly, the uncertainty for future climate change projections is high, especially for extreme weather events (IPCC, 2012).

The broader Mediterranean region is, according to observations and future climate projections, a hot spot of climate change (Diffenbaugh and Giorgi, 2012). This is mainly related to the fact that temperature and precipitation are changing in an opposite direction, intensifying environmental stress in the region (Lelieveld et al., 2012; Zittis et al., 2014a). In this type of arid, water-stressed environments improved knowledge and modelling of the hydrology is needed to provide better projections of the inflow of water to dams and of flood hazards, for the development of water allocation strategies, the sustainable exploitation of groundwater resources, and flood protection. Although a reduction in precipitation and prolonged droughts will likely be a most significant impact of climate change in the region, changes in extremes of rainfall are also expected (Paxian et al., 2015; Kitoh and Endo, 2016). These rare events, which can cause human casualties and significant infrastructure damage, are most of the times difficult to reproduce by models.

The horizontal grid spacing of current global climate models (typically100-200 km) is usually not sufficient for impact studies and further downscaling is required. The most crucial model components for rainfall generation are the parameterization schemes of convection and microphysical processes that occur on sub-grid scales. These processes in atmospheric models are empirically described either because the complexity and small scales involved make them too computationally expensive to be modeled or because there is insufficient knowledge about a specific process to represent it mathematically (Warner, 2011). The widely-used Weather Research and Forecasting (WRF) model has a large number of available schemes for the parameterization of each process, which can significantly alter the produced precipitation properties in terms of type, amounts or duration (Skamarock et al., 2008). One of the main reasons for these discrepancies is that different schemes were designed with different conceptual underpinnings and tunable parameters that are not universal and are also quite uncertain (Cossu and Hocke, 2014).

The objective of this study is to evaluate the performance of different convection and microphysics parameterizations of WRF, driven by reanalysis data, for the dynamic downscaling of precipitation extremes over Cyprus and the broader region of the eastern Mediterranean at 12-, 4- and 1-km resolution. Since there is no universal optimum setup, we test a large number of WRF configurations in order to investigate which ones are most skillful in reproducing five extreme precipitation events that have occurred over the region of interest. Each combination of four cumulus and five microphysics schemes was utilized while the rest of the model physics was identical. Our 20-member ensemble includes the Lin (Lin et al., 1983), WSM6 (Hong and Lim 2006), Thompson (Thompson et al., 2008), Ferrier (NOAA, 2001) and WDM6 (Lim and Hong, 2010) microphysics schemes and the Kain-Fritsch (Kain, 2004), Betts–Miller–Janjic (Janjic, 1994), Grell–Freitas (Grell and Freitas 2014) and Grell 3-D Ensemble (Grell and Devenyi, 2002) convection schemes. This selection was based on the performance of these schemes in similar applications such as the simulation of exceptionally extreme precipitation events (Luo et al., 2010; Tapiador et al. 2012; Mahbub Alam, 2014; Cassola et al., 2015; Meredith et al., 2015a; Remesan et al., 2015; Spiridonov et al., 2017), precipitation forecasting (Bukovsky et al., 2009; Clark et al., 2009; Ruiz and Saulo;

2010; Givati et al., 2012; Kioutsoukis et al., 2016) or climate applications (Evans et al., 2012; Soares et al., 2012; Ratna et al., 2014; Zittis et al., 2014; Katragkou et al., 2015). All simulations address a period of 15 days with the rainfall maximum more or less centered within this period. This might not be optimal for some applications, such as weather forecasting. However, we aim to investigate the model skill from a climate mode perspective, i.e. to reduce the dependence on initial conditions.

An increasing number of studies for various locations and types of experiments, and based on different regional models indicate a relatively realistic representation of precipitation processes in high-resolution convection-permitting simulations (Klemp, 2006; Prein et al., 2013; Cassola et al., 2015; Davolio et al., 2015; Fosser et al., 2015; Meredith et al., 2015b; Prein et al., 2015). Therefore, after applying an objective ranking scheme for identifying the best performing WRF configurations at 4-km resolution, we further downscaled them to 1-km to explore if convection-permitting simulations can reproduce the selected extreme precipitation events more accurately. Accordingly, we quantify the added value of each step of the downscaling.

When it comes to model evaluation the availability and quality of reference observations is of great importance, while it is especially critical for atmospheric variables such as precipitation that can significantly vary in space and time. The sparse network of available meteorological stations over the broader region highlights the issue of observational uncertainty (Gómez-Navarro et al., 2012; Tanarhte et al., 2012). In this context and for the same extreme cases we compare three state-of-the-art gridded observational datasets for the eastern Mediterranean region.

2. Data and Methodology

2.1 Model and Experimental Setup

For our simulations we used the version 3.7.1 of the WRF model. It was driven by the ERA-Interim (EI) reanalysis dataset (Simmons et al., 2006), which provides the initial and boundary conditions. The latter were updated every six hours. We used the one-way nesting option, downscaling EI (≈80 km) to 12 km (Domain 1: D01) and subsequently to 4 km (Domain 2: D02) and 1 km (Domain 3: D03). The three simulation domains are presented in Figure 1. The step between the forcing EI data and the coarse 12-km domain is well below the 10:1 ratio that is often referred as a maximum threshold for dynamical downscaling (Giorgi and Gutowski, 2015). Preliminary test simulations of the two-way nesting and nudging options were found not to improve the results for this particular experimental setup and weather events. In particular, we applied a full grid analysis nudging that was found not useful as it was pushing the simulations towards the generally drier ERA-Interim data, at least for the cases the latter was strongly underestimating precipitation. The model was set up with 40 vertical levels and a top at 50 hPa. To be useful for hydro-climatological applications, all model output was saved in hourly intervals. Interestingly, the duration of these simulations was found to be about 20% longer compared to the simulations where daily output was saved. This highlights the fact that input/output (I/O) processes during WRF simulations are not negligible and further optimization might be required.

As described in the Introduction section, our simulations ensemble is based on a combination of five microphysics and four convection parameterizations (Table 1). A brief description of these schemes follows:

Convection (Cumulus) Parameterizations:

- Kain-Fritsch (KF): Deep and shallow convection sub-grid scheme using a mass flux approach with updrafts, downdrafts, entrainment and detrainment processes.
- Betts-Miller-Janjic (BMJ): Column moist adjustment scheme, relaxing towards a well-mixed profile. No explicit updraft or downdraft and cloud detrainment.
- Grell-Freitas (GF): An improved stochastic parameterizations scheme that tries to smooth the transition to cloud-resolving scales. It includes explicit updrafts and downdrafts.
- Grell 3D (G3D) Ensemble scheme with explicit updrafts and downdrafts. It can also be used on high-resolution simulations as subsidence is spread to neighboring columns.

Cloud Microphysics Parameterizations:

- Lin: A sophisticated 5-class scheme (cloud water vapor, rain, ice, snow and graupel processes). It includes ice sedimentation and time-split fall terms. Suitable for real-data high-resolution simulations.
- WRF Single-Moment 6-class scheme (WSM6): A scheme with ice, snow and graupel processes suitable for high-resolution simulations.
- Thompson: A double-moment, 6-class scheme with ice, snow and graupel processes suitable for high-resolution simulations.
- Ferrier: A single-moment, 5-class, efficient scheme with diagnostic mixed-phase processes. It assumes that fractions of water and ice within the column are fixed during advection.
- WRF Double-Moment 6-class scheme (WDM6): Double moment 6-class scheme with graupel. Cloud condensation nuclei (CCN) and number concentration of cloud and rain are also predicted.

Besides the microphysics and cumulus parameterizations, our general configuration includes the Rapid Radiation Transfer Model (RRTMG) short and long-wave radiation (Iacono et al. 2008), the Mellor-Yamada-Janjic (MYJ) Planetary Boundary Layer scheme (Janjic, 1994), in addition to the Noah Land Surface Model (Tewari et al. 2004). Our WRF setup is similar to that of the Cyprus Department of Meteorology, used for operational weather forecasting (Tymvios et al., 2017), at least regarding the radiation and land surface model options. The 20 different setups were tested on the 12 and 4 km resolutions, while only the five best performing configurations were used to drive the 1-km simulations, since the computational cost of the latter was rather high. In this finer grid, the same microphysics scheme was used as for the selected 4-km driving model. However, convection was not parameterized but was explicitly resolved.

Table 1. Summary of the convection and microphysics parameterization options used for the 20 WRF configurations.

	WRF -1	WRF -2	WRF -3	WRF -4	WRF -5	WRF -6	WRF -7	WRF -8	WRF -9	WRF -10
CONVECTION	KF	KF	KF	KF	KF	BMJ	BMJ	BMJ	BMJ	BMJ
MICROPHYSICS	Lin	WSM6	Thompson	Ferrier	WDM6	Lin	WSM6	Thompson	Ferrier	WDM6
	WRF -11	**WRF -12**	**WRF -13**	**WRF -14**	**WRF -15**	**WRF -16**	**WRF -17**	**WRF -18**	**WRF -19**	**WRF -20**
CONVECTION	GF	GF	GF	GF	GF	G3D	G3D	G3D	G3D	G3D
MICROPHYSICS	Lin	WSM6	Thompson	Ferrier	WDM6	Lin	WSM6	Thompson	Ferrier	WDM6

2.2. Observational and Reanalysis Data

For evaluation of the model output we used a daily 1 X 1 km gridded precipitation dataset (Camera et al. 2014), hereafter called OBS. This dataset was derived from a dense network of 145 rain gauges, which covers the area of the island that is under the jurisdiction of the Republic of Cyprus and for the time period 1980-2010. For the purposes of this study, these gridded observations are considered to be the closest representation of reality. To perform a fair comparison between the three resolution nests we also interpolated OBS to the 12- and 4-km grids by applying a 4-point distance-weighted average spatial interpolation.

To obtain a representative picture of precipitation during the events in the broader region of the eastern Mediterranean we used three state-of-the-art, gridded daily observational datasets. These include version v.11.0 of the widely-used E-OBS dataset (Haylock et al. 2008), covering mainly Europe, and version V1101R1 of the APHRODITE's (Asian Precipitation - Highly-Resolved Observational Data Integration Towards Evaluation) daily gridded precipitation (Yatagai et al., 2012). Both have a horizontal grid spacing of 25 X 25 km. The coverage of APHRODITE for the Middle East and North Africa (MENA) region ends in 2007, thus, it was not available for the January 2010 extreme precipitation event. Additionally, we used the CHIRPS (Climate Hazards Group InfraRed Precipitation with Station data) dataset (Funk et al. 2015). The latter is a composite product of both satellite and station measurements and has a 5 X 5 km horizontal resolution, spanning a zone from 50°S to 50°N for all longitudes.

Since for this part of the world spatiotemporally consistent upper-air gridded observations either do not exist or are not publicly available, we utilized two reanalysis datasets to define the synoptic meteorological conditions during the selected extreme precipitation events. Besides the EI dataset, also used to provide initial and boundary conditions for our WRF simulations, we used geopotential values of the 500 hPa level derived from the NCEP-Reanalysis-2 dataset (Kanamitsu et al. 2002). The latter was provided by the Physical Science Division of the Earth System Research Laboratory/NOAA, from their web site at http://www.esrl.noaa.gov/psd/. We also used mean sea level pressure (MSLP) data from the same two reanalysis sources. These are considered to give a fair representation of reality as both surface and upper air observations were assimilated during the simulations.

Finally, to investigate the vertical structure of the atmosphere during the events we used temperature (T) and dew point temperature (Td) data from soundings. Unfortunately, this kind of information was not publicly available for Cyprus for the selected past events and therefore we used soundings from the adjacent station of Adana in southern Turkey and only for the 1994 and 2010 cases. The latter were available from the Department of Atmospheric Science of the University of Wyoming (http://weather.uwyo.edu/upperair/sounding.html).

2.3 Cyprus Climate and Description of Case Studies

According to the Köppen-Geiger climate classification (Peel et al., 2007), Cyprus is characterized by a warm temperate climate with hot and dry summers, typical for Mediterranean regions, while part of the island is classified as hot and arid. The mean annual precipitation in Cyprus is around 470 mm (Camera et al, 2016). Most water resources originate in the Troodos mountains, which cover nearly 60% of the island. This precipitation is essential for the fresh water supply of the country, as almost all rivers discharge into dammed areas. Troodos is a fractured igneous formation, and surface water flow and groundwater recharge are highly variable and strongly dependent

on the temporal and spatial distribution of precipitation. Moreover, flood events occurring in the mainland most of the times originate from these steeply sloping mountains.

Five extreme precipitation events of the recent past (1980-2010) were selected for this study (Table 2), based on precipitation and surface flow measurements on the northern side of the Troodos mountains. The 1988 and 1989 events were marked by high surface runoff in the watersheds along the northern slopes of the Troodos. The 1994 event was the largest 2-, 3-, 4-, and 5-day rainfall over Cyprus for the period 1980-2010; the 2005 event was a rare high summer rainfall, with extensive flooding in the capital city Nicosia; the 2010 event was the largest 1-day rainfall event over Cyprus. A brief discussion of the surface and middle troposphere conditions during the peaks of each of the five extreme weather events is presented in the Results section.

Table 2. Definition of the case studies and description of the extreme precipitation events.

	Simulation days	Season	Day of peak	Average Precipitation (mm) over Cyprus during peak day	Max. point precipitation (mm) during peak day	Average Monthly Precipitation (mm) over Cyprus (1980-2010)
Case 1988	17/12-31/12	Wet	24-Dec	55	126	104
Case 1989	02/01-16/01	Wet	09-Jan	50.1	144.6	98.1
Case 1994	12/11-26/11	Wet	21-Nov	47.8	140.7	62.4
Case 2005	25/05-08/06	Dry	31-May	11.2	115.4	17.4
Case 2010	11/01-25/01	Wet	18-Jan	66.5	162.5	98.1

2.4 Model Evaluation

2.4.1 Statistical Metrics and Ranking

To objectively assess if our WRF output is useful for hydro-climatological applications, we compared it with the high-resolution Cyprus observations by applying a set of relevant indices of extremes and efficiency metrics. These were applied on the daily model output and observations for each model grid point of Cyprus, and were then averaged. Our selection of evaluation metrics is summarized below.

The absolute error of the Maximum 5-day Precipitation Total ($RX5D_{ERROR}$) (Frich et al. 2002) is computed as follows:

$$\mathrm{RX5D_{ERROR}} = |\mathrm{RX5D_{OBS}}\text{-}\mathrm{RX5D_{SIM}}| \quad (1)$$

where *RX5D* is the maximum 5-day precipitation total during the two-week simulations and the subscripts OBS and SIM indicate the observed and simulated data. This five-day period is defined from the observations.

The absolute error of the Simple Daily Intensity Index (*SDII*) (Frich et al., 2002) is defined as:

$$SDII_{ERROR} = |SDII_{OBS}\text{-}SDII_{SIM}| \quad (2)$$

where SDII is the total precipitation over the period divided by the number of rainy days. Rainy days are defined as days with precipitation larger than 1mm.

The Percent Bias (*PBIAS*) measures the average tendency of the simulated values to be larger or smaller than their observed ones (Sorooshian et al. 1993):

$$PBIAS = 100\frac{\sum_{i=1}^{N}(SIM_i\text{-}OBS_i)}{\sum_{i=1}^{N} OBS_i} \quad (3)$$

where N is the number of simulation days times the number of grid cells.

The Nash-Sutcliffe efficiency (*NSE*) determines the relative magnitude of the residual variance ("noise") compared to the measured data variance ("information"). The modified *NSE* is not inflated by the squared values of the differences, because the squares in the original formula are replaced by absolute values (Krause et al., 2005). It ranges from –Infinitive to 1 (Perfect score =1). It is computed as follows:

$$mNSE = 1 - \frac{\sum_{i=1}^{N}|SIM_i\text{-}OBS_i|}{\sum_{i=1}^{N}|OBS_i\text{-}\overline{OBS}|} \quad (4)$$

The Kling-Gupta Efficiency (*KGE*) was developed by Gupta et al. (2009) to provide a diagnostically interesting decomposition of the Nash-Sutcliffe efficiency, which facilitates the analysis of the relative importance of its different components (correlation, bias and variability) in the context of hydrological modelling (Zambrano-Bigiarini, 2015). Kling et al. (2012) proposed a revised version, which was used in this study, to ensure that the bias and variability ratios are not cross-correlated. Kling-Gupta efficiencies range from minus infinity to one. Essentially, the closer to one, the more accurate the model. A more detailed description of this metric including the extended equations for calculation is presented in Zambrano-Bigiarini (2015).

The Modified Index of Agreement (*MIA*) is a standardized measure of the degree of the model prediction error. This index varies between 0 and 1. It was introduced by Willmott (1981) and refined by Legates and McCabe (1999) as follows:

$$MIA = 1 - \frac{\sum_{i=1}^{N}(OBS_i - SIM_i)}{\sum_{i=1}^{N}(|SIM_i - \overline{OBS}| + |OBS_i - \overline{OBS}|)} \quad (5)$$

Except for the *RX5D-error*, all metrics are computed over the full 15 days of the simulation. To select the five best performing WRF configurations out of the twenty and further proceed with the finer resolution (1-km) simulations, we performed an objective ranking based on the 4-km results (WRF-D02). We ranked all WRF configurations for each of the metrics described in the previous paragraphs and for each case study independently. Then we averaged the ranks for each configuration. The five configurations with the highest average ranking values (i.e. closest to 1) are considered to be the most realistic for the selected case studies. We refer to those as the five best configurations.

2.4.2 Added value of dynamical downscaling

To quantify the added value (AV) of our WRF dynamical downscaling in comparison with the global EI rainfall, we applied the method suggested by Di Luca et al. (2015). They quantified the AV by comparing a distance metric (d) between the global General Circulation Model (GCM) and the observations on one hand, and between the Regional Climate Model (RCM) simulation and the observations on the other, as follows:

$$AV = d(GCM, OBS) - d(RCM, OBS) \quad (6)$$

For our case the driving GCM is the ERA-Interim reanalysis dataset, while RCM refers to the WRF simulations for each of the three model nests. In order to have comparable results for all three WRF resolutions, we calculated the AV only over the five best-performing configurations that eventually drove the WRF-D03 1-km simulations. For this task, we used as distance metrics the six indices described in the previous section, applied similarly to the daily precipitation amounts. To compare AV results obtained from different climate statistics, we normalized the AV metrics by the sum of the RCM and GCM errors, according to Di Luca et al. (2016):

$$\widehat{AV}_d = \frac{d(GCM,OBS) - d(RCM,OBS)}{d(GCM,OBS) + d(RCM,OBS)} \quad (7)$$

The AV values vary between −1 and 1 with larger positive values suggesting smaller RCM errors than GCM errors and thus a higher added value from the RCM.

2.4.3 Synoptic conditions, precipitation maps and time-series

Maps of the simulated rainfall (3-day integrals centered on the peak of the events) were created for all five case studies. These are presented in the form of an ensemble mean over the five best WRF realizations and were compared with the different gridded precipitation datasets. Continuous daily time-series for the full length of each simulation were also produced to compare the WRF output with observations. Here we present time series for three representative stations in Cyprus, namely one located on south-west coast of the island (Pafos), one on the eastern peak of the Troodos mountains at an elevation of 1200 m above sea level (Kionia) and one inland low-elevation station (Nicosia).

Additionally, to explore the synoptic conditions during the events, we plotted the geopotential of the 500-hPa level and the mean sea level pressure based on the EI and NCEP reanalysis datasets. These plots are of a larger domain in order to obtain a more general picture of the circulation during the peak days of the events. They are compared with the 500-hPa geopotential and mean sea level pressure derived from our five best WRF simulations for the 12-km domain. Finally, we investigated if the vertical structure of the atmosphere is adequately reproduced by the model simulations. For the two cases with available data (1994 and 2010) we used the 12:00 UTC sounding of the peak rainfall day of the events and we compared it with the closest grid point of our 4-km WRF output (WRF-D02).

The above results are presented here for two (1994 and 2010) out of the five case studies, while the other three are presented in the supplementary material. These two cases are representative of a successful and a problematic downscaling case.

3. Results

3.1 Selection of best configuration

Figure 2 summarizes the results of the ranking of the 20 WRF setups. This was based on the six skill metrics of the 4-km WRF-D02 simulations of all five extreme events (Table S2 of the supplementary material). The ranking among all simulations is presented in the upper panel of this figure, while in the bottom panel we show the ranking of clusters of the same convection and microphysics parameterization schemes. Simulations that utilized the G3D convection and Lin microphysics (WRF configurations: 1, 6, 11, 16, 17, 18, 19, 20) were found to poorly reproduce the five rainfall events, as indicated by the performance metrics. We found a clear advantage in the simulations of extreme precipitation when BMJ and GF convection schemes were used in a combination with Ferrier, WDM6 and WSM6 microphysics (WRF configurations: 7, 9, 10, 12 and 14). These are the five best model configurations that were used for the 1-km simulations. In agreement with our findings, a number of physics intercomparison studies also indicated that the Betts-Miller-Janjic scheme outperforms in terms of precipitation simulation (Ishak et al., 2012; Evans et al., 2012; Ratna et al., 2014; Remesan et al., 2015). Similarly, the WRF Single and Double Moment schemes (WSM, WDM) and Ferrier were found to be more accurate (Evans et al., 2012; Givati et al., 2012; Remesan et al., 2015; Kioutsoukis et al., 2016). The performance metrics of all WRF simulations are presented in Tables S1-S3 of the supplementary material.

3.2 Model resolution and added value

In Table 3 we present a summary of the performance metrics for the EI and three WRF nests versus the Cyprus high-resolution observations, averaged for each case study. For most case studies and performance metrics the dynamical downscaling with WRF improves the EI precipitation. Exceptions are all quantitative metrics (RX5D error, SDII error and PBIAS) for the December 1988 case and PBIAS for the January 2010 case. Interestingly, for these two events the efficiency metrics (mNSE, KGE and MIA) improved with the downscaling, despite the fact that the precipitation amounts did not.

As the PBIAS metric indicates, our WRF simulations tend to underestimate the amount of precipitation over Cyprus during the majority of the simulations. An exception is the very localized June 2005 event, where the model overestimates precipitation in general. The more detailed Table S1 of the supplementary material indicates that this overestimation of the rainfall amounts during the 2005 event is strongest when the GF and G3D ensemble schemes of convection parameterization are used. This behavior is evident only in the summer case and may suggest a poorer ability of the aforementioned schemes to correctly reproduce warm season thermally driven convection, at least for the case of Cyprus or similar environments, and needs further investigation.

The efficiency and agreement indices have generally positive values that are closest to 1 for the January 1989 and November 1994 cases.

Table 3. Statistical evaluation metrics for each case study between the Cyprus precipitation observations and EI, WRF-D01 (12 km), WRF-D02 (4 km) and WRF-D03 (1 km). Stars (*) indicate the cases where only the five-best configurations were considered.

	RX5D error (perfect=0)					SDII error (perfect=0)					PBIAS (perfect=0)				
case:	**1988**	**1989**	**1994**	**2005**	**2010**	**1988**	**1989**	**1994**	**2005**	**2010**	**1988**	**1989**	**1994**	**2005**	**2010**
EI	**34.7**	59.2	101	27.5	66.7	**10.1**	12.8	12.8	6.4	8.5	**2.2**	-37.8	-32.7	29.0	**-46.5**
D01	56.6	50.8	97.2	22.8	76.5	12.8	8.3	12.1	5.6	9.1	-48.7	-31.6	-16.7	137.3	-62.1
D02	58.7	44.9	73.8	25.6	70.2	12.2	8.2	10.1	5.7	8.7	-46.8	-15.5	-9.6	186.4	-57.6
D02*	58.9	38.0	57.3	21.7	72.2	12.3	7.0	8.6	5.0	8.7	-57.8	-16.9	-16.6	32.9	-62.7
D03*	40.7	**23.5**	**44.0**	**13.0**	**56.0**	10.9	**4.7**	**5.5**	**3.7**	**3.3**	-51.4	**-9.6**	**4.4**	**-22.3**	-47.5
	mNSE (perfect =1)					**KGE (perfect=1)**					**MIA (perfect =1)**				
case:	**1988**	**1989**	**1994**	**2005**	**2010**	**1988**	**1989**	**1994**	**2005**	**2010**	**1988**	**1989**	**1994**	**2005**	**2010**
EI	0.02	0.31	0.32	-0.06	0.13	-0.12	0.29	0.34	**-0.34**	-0.24	0.50	0.58	0.58	0.54	0.57
D01	0.36	0.52	0.36	-0.71	0.25	0.07	0.51	0.32	-1.20	-0.06	0.64	0.74	0.67	0.50	0.57
D02	0.36	0.50	0.38	-1.05	0.26	0.08	0.50	0.41	-1.65	-0.03	0.63	0.74	0.68	0.51	0.58
D02*	0.41	0.53	0.46	-0.14	**0.30**	0.06	0.55	0.51	-0.41	-0.04	0.65	0.76	0.71	**0.55**	**0.59**
D03*	**0.42**	**0.71**	**0.42**	**0.01**	0.24	**0.12**	**0.72**	**0.56**	-0.39	**0.12**	**0.66**	**0.85**	**0.72**	0.54	**0.59**

The results of the added value analysis, averaged over the five events, are presented in Table 4. We found that, on average, all three subsequent downscaling steps added some value to the EI precipitation data. In general, the added value was found to be more significant in terms of model efficiency than for the precipitation amounts as the higher normalized AV metrics of Table 4 indicate. Similar as other studies (Prein et al., 2013; Meredith et al., 2015), we found that the further increase of the horizontal resolution and the explicit treatment of convection processes, which was the case for the 1-km simulations, increased the added value.

Table 4. Added value of the WRF dynamical downscaling, averaged for the five extreme precipitation events and for each distance and efficiency metric.

Added Value (AV)	RX5D error	SDII error	PBIAS	mNSE	KGE	MIA
EI vs. WRF 12km	0.08	0.01	-0.11	0.29	0.55	0.09
EI vs. WRF 4km	0.08	0.1	0.03	0.38	0.86	0.1
EI vs. WRF 1km	0.24	0.29	0.1	0.43	0.92	0.12

To explore the performance of the high-resolution simulations, we present a case by case comparison between the detailed gridded observations over Cyprus and the 4- and 1-km simulations (Figure 3). These maps display results averaged over the five best WRF configurations. For the 1988 event, the 1-km simulation results (WRF-D03) were closer to the observations than the 4-km simulations (WRF-DO2), but still both the WRF-D02 and WRF-D03 runs strongly underestimated this event. For the January 1989 case, WRF-D03 is found to outperform WRF-D02, especially over the central Troodos mountains, while it is found to overestimate the event for the western part of the island, which is dominated by the slopes of the Troodos mountains. This is also the case for the November 1994 event, but the D03 precipitation is closer to the observations for the central-east part of the Troodos mountains. For these two events WRF-D02 is found to perform better for the flat, southeast part of the island, where WRF-D03 overestimates precipitation. For the late spring 2005 event the 4-km runs (WRF-D02) are found to better capture rainfall over the eastern part of the island, while they missed the very localized

precipitation center that was observed between the Nicosia and Kionia stations. The latter, slightly displaced, was simulated only by the convection-permitting 1-km runs. Finally, the January 2010 event was not very well reproduced by either the WRF-D02 or WRF-D03 simulations. However, the 4-km runs reproduced some rainfall over the southeast part of Cyprus that was absent in the 1-km runs. The added value of downscaling to convection-permitting simulations is also found to be a question of location. Nevertheless, for these case studies, the improvement is most significant over complex, high-elevation terrains.

3.3 Synoptic conditions, precipitation maps and time-series

Case: November 1994

This extreme precipitation event occurred between the 20th and 22nd of November 1994. This is the only autumn event from the five selected case studies. According to the two reanalysis datasets (EI and NCEP), it was a result of an upper air trough of north-east to south-west direction extended from the southern Balkans towards the north coast of Africa. As depicted in the top row panels of Figure 4, it approached Cyprus from the west. Similar conditions prevailed also during the 1988 and 1989 case studies, which are presented in detail in the supplementary material.

A tear-off upper level low within the ridge was also formed over the eastern Mediterranean. Noteworthy, this is a pattern commonly connected with significant precipitation amounts over Cyprus (Tymvios et al. 2010). As a result, low pressure surface conditions prevailed ahead of the upper air trough (Figure 4 – bottom row). This surface depression that caused the extreme rainfall during the event was found to be well captured by our WRF simulations (Figures 4c and 4f).

Figure 5 (left panel) depicts the observed and modeled vertical structure of the atmosphere in terms of temperature and dew point temperature during the peak day of the event. Since there was no information available over Cyprus we used data from the adjacent station of Adana in south Turkey, which was also strongly affected by the event. For this particular case WRF (purple curves) is found skillful in reproducing the observed conditions (blue lines) for the part of the atmosphere for which we have information from the sounding. For WRF we present the ensemble mean of the five best configurations of the 12-km simulations. The convergence of the temperature and dew point temperature curves around the 700-500 hPa levels indicates that high availability of water content is evident in both observations and model output, while other features such as the level of the tropopause are also accurately simulated.

This low-pressure system resulted in 3-day precipitation totals of more than 200 mm locally and it mostly affected south Turkey and much of the coastal areas in the Levant (Figure 6). CHIRPS precipitation (Figure 6g-h) is found to be exaggerated compared to the other observational datasets in most of the study region including Cyprus. However, CHIRPS does not include precipitation over the eastern Mediterranean coast (Israel, Lebanon, Syria), which happens to be the case for E-OBS and, to a lesser extent, APHRODITE (Figure 6c-f).

More regionalized information for Cyprus can be found in the panels of Figure 7. Precipitation of EI is found again very homogeneous and underestimates the observed rainfall for large parts of the island (Figure 7a). Generally, CHIRPS underestimates the event over most of the area of the island. On the other hand, our 1-km WRF-D03 simulation reproduces the precipitation amount during the November 1994 event relatively well (Figure 7d). However, some displacement of the location of the rainfall peaks is evident. In the gridded observations (Figure

7c) the event is found to be centered around Kionia station, however, the simulation results in a westward shift of precipitation. Additional information for the whole extent of the simulation can be found in the indicative time-series plots of Figure 8 that indicate a reasonable correlation between the observed and modelled rainfall. A smaller precipitation event during the first days of the simulations, most pronounced at the Pafos station (Figure 8 – left column), was also reasonably well reproduced by the model.

Case: January 2010

This is the most recent event that was simulated in this study. The rainfall peak was observed on the 18th of January 2010 and it mainly affected eastern Turkey and the Levant coast. Figure 9 depicts the synoptic conditions during the peak of the event according to the EI and NCEP reanalysis and WRF simulations. An upper-air trough over the eastern Mediterranean is again the prevailing synoptic feature in the region (Figure 8 – top row). However, this trough has somehow different properties than the November 1994 event, as its axis follows a north-west to south-east direction. This results in a surface pressure depression of the form of a tear-off low that affects large parts of the eastern Mediterranean and the Middle East (Figure 9 – bottom row). Broadly speaking the WRF simulations reproduced the main synoptic features during the event (Figure 9c). The center of low pressure at the surface is found at the east of the island of Cyprus (Figure 9f). The model broadly captured the atmospheric vertical structure (Figure 5 – right panel). Nevertheless, some discrepancies from the sounding observations are found near the surface for temperature and in the lower levels of the stratosphere for dew point temperature.

Similar as the previous case study (and the events presented in the supplementary material), CHIRPS is found to be wettest (Figures 10e and 10f). In particular, over Lebanon and west Cyprus this dataset indicates precipitation of the order of 200 mm for the period 17-19/01/2010 while considerable rainfall amounts are also indicated over most of the eastern Mediterranean coast. This is much more than reported by E-OBS and simulated by EI, high-lighting again the issue of observational uncertainty. The APHRODITE dataset for the Middle East region does not cover 2010. Our WRF simulations (Figures 10g and 10h) seem to generate precipitation over the eastern coast of the Mediterranean and the eastern parts of Turkey while they fail to reproduce the high rainfall over Cyprus for this extreme event.

In more detail for Cyprus, the high-resolution observations for this event report precipitation amounts of about 100 mm for the whole island with localized centers, mainly over the northern slopes of the Troodos mountains, where precipitation exceeds 150 mm (Figure 11c). The EI dataset (Figure 11a) strongly underestimated this, while CHIRPS strongly overestimates precipitation over the western part of the island (Figure 11b). For the 3-day period around the peak of the event the 1-km WRF-D03 simulations are much drier and only over some parts of Cyprus some scattered precipitation is generated.

The evolution of precipitation during the two weeks of simulation for this event is presented in Figure 12. As discussed in the previous paragraph, WRF fails to reproduce this extreme event. Nevertheless, it captured the two smaller-scale events that occurred in the beginning and towards the end of the simulation period.

4. Conclusions

We investigated the WRF model performance in 20 combinations of convection and microphysical parameterization schemes for five extreme precipitation events over the eastern Mediterranean region. Based on an objective ranking process, we found that the BMJ and GF convection schemes reproduce these events most accurately, while the model performance was best when the Ferrier, WDM6 and WSM6 microphysics parameterizations were used. Our findings can be used as a point of reference for the simulation of precipitation extremes over the region of interest. While we used a large number of parameterizations we did not exhaust all available options. Yet, this ranking can be used as a reference for WRF users interested in similar type of environments and weather phenomena.

Our results show that dynamical downscaling with the high-resolution WRF model improves the EI rainfall patterns for the eastern Mediterranean region, at least for three out of five extreme precipitation events (1989, 1994 and 2005 cases) in terms of rainfall amounts and timing. Statistical analysis reveals that results of the two higher-resolution domains (4 and 1-km) are consistently closer to the observations. Although the simulation was not nudged to the driving reanalysis dataset, for most of the tested events WRF was able to reproduce the synoptic conditions that resulted in the extreme precipitation. The modeled rainfall was generally very well synchronized with the observations, which is not always expected in non-nudged hindcast simulations of such duration. Even for the events where the downscaling did not improve the EI precipitation total amounts (cases 1988 and 2010) the timing of the events was more accurate as indicated by the higher efficiency indices after the downscaling.

In agreement with the literature, the added value of the downscaling is found higher between the EI and the 1-km nest. These convection-resolving simulations are found to outperform the lower resolution versions, especially over the high elevation regions that are most critical for the water resources of the island, as they control the flow to the major dams. Nevertheless, for some parts of Cyprus precipitation was better simulated by the 4-km nest, highlighting the need for further research on the advantage of convection-permitting simulations.

Interestingly, we found large discrepancies between three state-of-the-art gridded observational datasets during the tested extreme precipitation events. Our findings indicate that E-OBS and APHRODITE precipitation is systematically lower than CHIRPS over the broader eastern Mediterranean region. Accordingly, for the cases considered in Cyprus the two former datasets strongly underestimate the precipitation reported from the high-density station network. While CHIRPS might be useful in providing a general overview of precipitation on the large scale, we found large deviations from the high-resolution observations over Cyprus. This is probably related to the small number of stations that were utilized for the construction of this dataset over the island (Katsanos et al. 2016).

To reduce observational uncertainty and increase the confidence of climate studies over the eastern Mediterranean and Middle East region, we strongly encourage local data holders (e.g. state hydro-meteorological services, universities, research institutions), to open access to their data for scientific use. In the same context, we recommend the use of multiple sources of observations for model validation.

Acknowledgments The BINGO project has received funding from the European Union's Horizon 2020 Research and Innovation programme, under the Grant Agreement number 641739. This work was supported by the Cy-Tera Project (NEA ΥΠΟΔΟΜΗ/ΣΤΡΑΤΗ/0308/31), which is co-funded by the European Regional Development Fund and the Republic of Cyprus

484 through the Research Promotion Foundation. We acknowledge the E-OBS dataset from the EU-FP6 project ENSEMBLES (http://en-
485 sembles-eu.metoffice.com) and the data providers in the ECA&D project (http://www.ecad.eu). We also acknowledge the Cyprus
486 Department of Meteorology for providing their precipitation data.
487
488

489 References

490 Camera, C., Bruggeman, A., Hadjinicolaou P., Pashiardis, S., Lange, M.A., 2014. Evaluation of interpolation techniques for the cre-
491 ation of gridded daily precipitation (1×1 km2); Cyprus, 1980–2010. Journal of Geophysical Research, Atmospheres,
492 119(2):2013JD020611+

493 Camera, C., Bruggeman, A., Hadjinicolaou, P., Michaelides, S., Lange, M. A., 2016. Evaluation of a spatial rainfall generator for
494 generating high resolution precipitation projections over orographically complex terrain. Stochastic Environmental Research and Risk
495 Assessment, (First Online), doi: 10.1007/s00477-016-1239-1

496 Cassola, F., Ferrari, F., Mazzino, A., 2015. Numerical simulations of Mediterranean heavy precipitation events with the WRF model:
497 A verification exercise using different approaches. Atmospheric Research 164–165, 210-225, doi: http://dx.doi.org/10.1016/j.at-
498 mosres.2015.05.010

499 Clark, A. J., Gallus, W. A., Xue, M., Kong, F., 2009. A comparison of precipitation forecast skill between small Convection-Allowing
500 and large Convection-Parameterizing ensembles. Weather Forecasting, 24(4), 1121-1140, doi: 10.1175/2009waf2222222.1

501 Collins, M., Knutti R., Arblaster J., Dufresne J.-L., Fichefet T., Friedlingstein P., Gao X., Gutowski W.J., Johns T., Krinner G.,
502 Shongwe M., Tebaldi C., Weaver A. J. Wehner M., 2013. Long-term Climate Change: Projections, Commitments and Irreversibility.
503 In: Climate Change 2013: The Physical Science Basis. Contribution of Working Group I to the Fifth Assessment Report of the Inter-
504 governmental Panel on Climate Change [Stocker, T.F., Qin D., Plattner G.-K., Tignor M., Allen S.K., Boschung J., Nauels A., Xia
505 Y., Bex V. and Midgley P.M. (eds.)]. Cambridge University Press, Cambridge, UK and New York, NY, USA.

506 Cossu, F., Hocke, K., 2014. Influence of microphysical schemes on atmospheric water in the weather research and forecasting model.
507 Geoscientific Model Development, 7, 147-160, doi: 10.5194/gmd-7-147-2014

508 Davolio, S., Silvestro, F., Malguzzi, P., 2015. Effects of increasing horizontal resolution in a Convection-Permitting model on flood
509 forecasting: The 2011 dramatic events in Liguria, Italy. Journal of Hydrometeorology, 16(4), 1843-1856, doi: 10.1175/jhm-d-14-
510 0094.1

511 Di Luca, A., de Elía, R., Laprise, R., 2015. Challenges in the quest for added value of regional climate dynamical downscaling. Current
512 Climate Change Reports 1(1), 10-21, doi: 10.1007/s40641-015-0003-9

513 Di Luca, A., Argüeso, D., Evans, J. P., de Elía, R., Laprise, R., 2016. Quantifying the overall added value of dynamical downscaling
514 and the contribution from different spatial scales. Journal of Geophysical Research: Atmospheres, 121(4), 1575-1590, doi:
515 10.1002/2015jd024009

516 Diffenbaugh, N., Giorgi, F., 2012. Climate change hotspots in the CMIP5 global climate model ensemble. Climatic Change, 114(3-
517 4), 813-822.

518 Evans, J., Ekström, M., Ji, F., 2012. Evaluating the performance of a WRF physics ensemble over South-East Australia. Climate
519 Dynamics, 39(6):1241-1258, doi: 10.1007/s00382-011-1244-5

520 Fosser, G., Khodayar, S., Berg, P., 2015. Benefit of convection permitting climate model simulations in the representation of convec-
521 tive precipitation. Climate Dynamics 44(1-2), 45-60, doi: 10.1007/s00382-014-2242-1

522 Frich P., Alexander, L.V., Della-Marta, P., Gleason, B., Haylock, M., Klein Tank, A.M.G., Peterson T., 2002. Observed coherent
523 changes in climatic extremes during the second half of the twentieth century. Climate Research, 19(3), 193-212.

Funk, C., Peterson, P., Landsfeld, M., Pedreros, D., Verdin, J., Shukla, S., Husak G., Rowland J., Harrison L., Hoell, A., Michaelsen, J., 2015. The climate hazards infrared precipitation with stations—a new environmental record for monitoring extremes. Scientific Data, 2, 150066, doi:10.1038/sdata.2015.66

Giorgi, F., Gutowski, W.J., 2015. Regional dynamical downscaling and the CORDEX initiative. Annual Review of Environment and Resources, 40(1), 467-490, doi: 10.1146/annurev-environ-102014-021217

Givati, A., Lynn, B., Liu, Y., Rimmer, A., 2012. Using the WRF model in an operational streamflow forecast system for the Jordan river. Journal of Applied Meteorology and Climatology, 51(2), 285-299.

Gómez-Navarro, J.J., Montávez, J.P., Jerez, S., Jiménez-Guerrero, P., Zorita, E., 2012. What is the role of the observational dataset in the evaluation and scoring of climate models? Geophysical Research Letters, 39(24), L24701, doi: 10.1029/2012GL054206

Gupta, H. V., Kling, H., Yilmaz, K. K., Martinez, G. F., 2009. Decomposition of the mean squared error and NSE performance criteria: Implications for improving hydrological modelling. Journal of Hydrology, 377(1-2):80-91.

Grell, G. A, Devenyi, D., 2002. A generalized approach to parameterizing convection combining ensemble and data assimilation techniques. Geophysical Research Letters, 29, 1693.

Grell, G.A., Freitas, S.R., 2014. A scale and aerosol aware stochastic convective parameterization for weather and air quality modeling. Atmospheric Chemistry and Physics, 14, 5233-5250, doi:10.5194/acp-14-5233-2014

Haylock, M.R., Hofstra, N., Klein Tank, A.M.G., Klok, E.J., Jones P.D., New M., 2008. A European daily high-resolution gridded dataset of surface temperature and precipitation. Journal of Geophysical Research, Atmospheres, 113, D20119, doi:10.1029/2008JD10201

Hong, S.Y., Lim J.O.J., 2006. The WRF single–moment 6–class microphysics scheme (WSM6). Journal of the Korean Meteorological Society, 42, 129–151.

Iacono, M. J., Delamere, J.S., Mlawer, E.J., Shephard, M.W., Clough, S.A., Collins, W.D., 2008. Radiative forcing by long–lived greenhouse gases: Calculations with the AER radiative transfer models. Journal of Geophysical Research, Atmospheres, 113, D13103.

IPCC, 2012: Summary for Policymakers. In: Managing the Risks of Extreme Events and Disasters to Advance Climate Change Adaptation [Field, C.B., V. Barros, T.F. Stocker, D. Qin, D.J. Dokken, K.L. Ebi, M.D. Mastrandrea, K.J. Mach, G.-K. Plattner, S.K. Allen, M. Tignor, and P.M. Midgley (eds.)]. A Special Report of Working Groups I and II of the Intergovernmental Panel on Climate Change. Cambridge University Press, Cambridge, UK, and New York, NY, USA, pp. 1-19.

Ishak, A. M., Bray, M., Remesan, R., Han, D., 2012. Seasonal evaluation of rainfall estimation by four cumulus parameterization schemes and their sensitivity analysis. Hydrol. Process., 26(7):1062-1078. doi:10.1002/hyp.8194

Janjic, Z.I., 1994. The Step–Mountain Eta Coordinate Model: Further developments of the convection, viscous sublayer, and turbulence closure schemes. Monthly Weather Review, 122, 927–945.

Kain, J.S., 2004. The Kain–Fritsch convective parameterization: An update. Journal of Applied Meteorology, 43, 170–181.

Kanamitsu, M., Ebisuzaki, W., Woollen, J., Yang, S.-K., Hnilo, J. J., Fiorino, M., and Potter, G. L. (2002). NCEP–DOE AMIP-II reanalysis (r-2). Bull. Amer. Meteor. Soc., 83(11):1631-1643. DOI: 10.1175/bams-83-11-1631

Katragkou, E., García-Díez, M., Vautard, R., Sobolowski, S., Zanis, P., Alexandri, G., Cardoso, R.M., Colette, A., Fernández, J., Gobiet, A., Goergen, K., Karacostas, T., Knist, S., Mayer, S., Soares, P.M.M., Pytharoulis, I., Tegoulias, I., Tsikerdekis, A., Jacob, D., 2015. Hindcast regional climate simulations within EURO-CORDEX: evaluation of a WRF multi-physics ensemble. Geoscientific Model Development, 8, 603-618, doi:10.5194/gmd-8-603-2015

Katsanos, D., Retalis, A., Michaelides, S., 2016. Validation of a high-resolution precipitation database (CHIRPS) over Cyprus for a 30-year period. Atmospheric Research, 169, 459-464, doi: 10.1016/j.atmosres.2015.05.015

Kioutsioukis, I., de Meij, A., Jakobs, H., Katragkou, E., Vinuesa, J.-F., Kazantzidis, A., 2016. High resolution WRF ensemble forecasting for irrigation: Multi-variable evaluation. Atmospheric Research, 167, 156-174, doi: 10.1016/j.atmosres.2015.07.015

Kitoh, A., Endo, H., 2016. Changes in precipitation extremes projected by a 20-km mesh global atmospheric model. Weather and Climate Extremes, 11, 41-52, doi: 10.1016/j.wace.2015.09.001

Klemp, J.B., 2006. Advances in the WRF model for convection-resolving forecasting. Advances in Geosciences, 7, 25-29. doi:10.5194/adgeo-7-25-2006

Kling, H., Fuchs, M., Paulin, M., 2012. Runoff conditions in the upper Danube basin under an ensemble of climate change scenarios. Journal of Hydrology, 424-425, 264-277.

Krause P., Boyle, D.P., Bäse, F., 2005. Comparison of different efficiency criteria for hydrological model assessment, Advances in Geosciences, 5, 89-97.

Legates, D.R., McCabe, G.J., 1999. Evaluating the Use of "Goodness-of-Fit" Measures in Hydrologic and Hydroclimatic Model Validation. Water Resources Research, 35, 233-241.

Lelieveld, J., Proestos, P., Hadjinicolaou, P., Tanarhte, M., Zittis, G., 2016. Strongly increasing heat extremes in the Middle East and North Africa (MENA) in the 21st century. Climatic Change, 137, 145-160, doi: 10.1007/s10584-016-1665-6

Lim, K.S.S., Hong, S.Y., 2010. Development of an effective double–moment cloud microphysics scheme with prognostic cloud condensation nuclei (CCN) for weather and climate models. Monthly Weather Review, 138, 1587–1612.

Lin, Y.L., Farley, R.D., Harold, D. O., 1983. Bulk Parameterization of the Snow Field in a Cloud Model. Journal of Applied Meteorology and Climatology, 22, 1065–1092.

Mahbub Alam, M., 2014. Impact of cloud microphysics and cumulus parameterization on simulation of heavy rainfall event during 7–9 October 2007 over Bangladesh. Journal of Earth System Science, 123(2), 259-279, doi: 10.1007/s12040-013-0401-0

Meredith, E.P., Maraun, D., Semenov, V.A., Park, W. 2015a. Evidence for added value of convection-permitting models for studying changes in extreme precipitation. Journal of Geophysical Research, Atmospheres, 120(24), 2015JD024238+.

Meredith, E.P., Semenov, V.A., Maraun, D., Park, W., Chernokulsky, A.V., 2015b. Crucial role of black sea warming in amplifying the 2012 Krymsk precipitation extreme. Nature Geoscience, 8(8), 615-619 doi: 10.1038/ngeo2483

Michaelides, S.C., Tymvios, F.S., Michaelidou, T., 2009. Spatial and temporal characteristics of the annual rainfall frequency distribution in Cyprus. Atmospheric Research, 94(4), 606-615, doi: 10.1016/j.atmosres.2009.04.008

NOAA, National Oceanic and Atmospheric Administration, 2001. Changes to the NCEP Meso Eta Analysis and Forecast System: Increase in resolution, new cloud microphysics, modified precipitation assimilation, modified 3DVAR analysis. (Available online at http://www.emc.ncep.noaa.gov/mmb/mmbpll/eta12tpb/.)

Paxian, A., Hertig, E., Seubert, S., Vogt, G., Jacobeit, J., Paeth, H., 2015. Present-day and future Mediterranean precipitation extremes assessed by different statistical approaches. Climate Dynamics, 44(3-4), 845-860, doi: 10.1007/s00382-014-2428-6

Peel, M.C., Finlayson, B.L., McMahon, T.A., 2007. Updated world map of the Köppen-Geiger climate classification. Hydrology and Earth System Sciences, 11(5), 1633-1644, doi: 10.5194/hess-11-1633-200

Prein, A.F., Gobiet, A., Suklitsch, M., Truhetz, H., Awan, N. K., Keuler, K., Georgievski, G., 2013. Added value of convection permitting seasonal simulations. Climate Dynamics, 41(9), 2655-2677, doi: 10.1007/s00382-013-1744-6

Prein, A.F., Langhans, W., Fosser, G., Ferrone, A., Ban, N., Goergen, K., Keller, M., Tölle, M., Gutjahr, O., Feser, F., Brisson, E., Kollet, S., Schmidli, J., van Lipzig, N.P.M., Leung, R., 2015. A review on regional convection-permitting climate modeling: Demonstrations, prospects, and challenges. Reviews of Geophysics, 53(2), 323-361. doi:10.1002/2014rg000475

Ratna, S., Ratnam, J. V., Behera, S. K., Rautenbach, Ndarana, T., Takahashi, K., Yamagata, T., 2014. Performance assessment of three convective parameterization schemes in WRF for downscaling summer rainfall over south Africa. Climate Dynamics 42(11-12):2931-2953, doi: 10.1007/s00382-013-1918-2

Remesan, R., Bellerby, T., Holman, I., Frostick, L., 2015. WRF model sensitivity to choice of parameterization: a study of the 'York flood 1999'. Theoretical and applied climatology, 122(1-2):229-247, doi: 10.1007/s00704-014-1282-0

Simmons, A., Uppala, S., Dee, D., Kobayashi, S., 2006. ERA-Interim: New ECMWF Reanalysis Products from 1989 Onwards. ECMWF Newsletter, 110, 26-35.

Skamarock, W.C. et al., 2008, A description of the Advanced Research WRF version 3. NCAR Tech. Note NCAR/TN-4751STR

Sorooshian, S., Duan, Q., Gupta, V.K., 1993. Calibration of rainfall-runoff models: Application of global optimization to the Sacramento soil moisture accounting model. Water Resources Research, 29(4), 1185-1194, doi: 10.1029/92WR02617

Spiridonov, V., Baez, J., Telenta, B., 2017. Heavy convective rainfall forecast over Paraguay using coupled WRF-Cloud Model. In Perspectives of Atmospheric Sciences, Karacostas T., Bais A., Nastos P.T. (editors), pp183-189, ISBN: 978-3-319-35095-0, doi: 10.1007/978-3-319-35095-0_22

Tanarhte, M., Hadjinicolaou, P., Lelieveld, J., 2012. Intercomparison of temperature and precipitation data sets based on observations in the Mediterranean and the Middle East. Journal of Geophysical Research, Atmospheres, 117(D12), D12102+, doi: 10.1029/2011jd017293

Tapiador, F.J., Tao, W.K., Shi, J.J., Angelis, C.F., Martinez, M.A., Marcos, C., Rodriguez, A., Hou, A., 2012. A comparison of perturbed initial conditions and multiphysics ensembles in a severe weather episode in Spain. Journal of Applied Meteorology and Climatology, 51(3), 489-504, doi: http://dx.doi.org/10.1175/JAMC-D-11-041.1

Thompson, G., Field, P.R., Rasmussen, R.M., Hall, W.D., 2008. Explicit forecasts of winter precipitation using an improved Bulk Microphysics Scheme. Part II: Implementation of a new snow parameterization. Monthly, Weather, Review, 136, 5095–5115, doi: http://dx.doi.org/10.1175/2008MWR2387.1

Tymvios, F., Savvidou, K., Michaelides, S.C., 2010. Association of geopotential height patterns with heavy rainfall events in Cyprus. Advances in Geosciences, 23, 73-78, doi: 10.5194/adgeo-23-73-2010

Tymvios, F., Charalambous, D., Lelieveld, J., Michaelides, S., 2017. Comparative forecasts of a Local Area Model (WRF) in summer for Cyprus. In Perspectives of Atmospheric Sciences, Karacostas T., Bais A., Nastos P.T. (editors), pp151-157, ISBN: 978-3-319-35095-0, doi: 10.1007/978-3-319-35095-0_22

Warner, T.T., 2011. Numerical Weather and Climate Prediction. Cambridge University Press, Cambridge, UK, pp 526

Willmott, C.J., 1981. On the Validation of Models. Physical Geography, 2, 184-194.

Yatagai, A., Kamiguchi, K., Arakawa, O., Hamada, A., Yasutomi, N., Kitoh, A., 2012. APHRODITE: Constructing a Long-Term daily gridded precipitation dataset for Asia based on a dense network of rain gauges. Bulletin of the American Meteorological Society, 93(9), 1401-1415, doi: 10.1175/bams-d-11-00122.1.

Zambrano-Bigiarini, M., 2015. Goodness-of-fit functions for comparison of simulated and observed hydrological time series. A description of the HydroGOF R package (https://cran.r-project.org/web/packages/hydroGOF/hydroGOF.pdf)

Zittis, G., Hadjinicolaou, P., Lelieveld, J., 2014a. Role of soil moisture in the amplification of climate warming in the eastern Mediterranean and the Middle East. Climate Research, 59(1), 27-37, doi:10.3354/cr01205

Zittis, G., Hadjinicolaou, P., Lelieveld, J., 2014b. Comparison of WRF model physics parameterizations over the MENA-CORDEX domain. American Journal of Climate Change, 3, 490-511, doi: 10.4236/ajcc.2014.35042

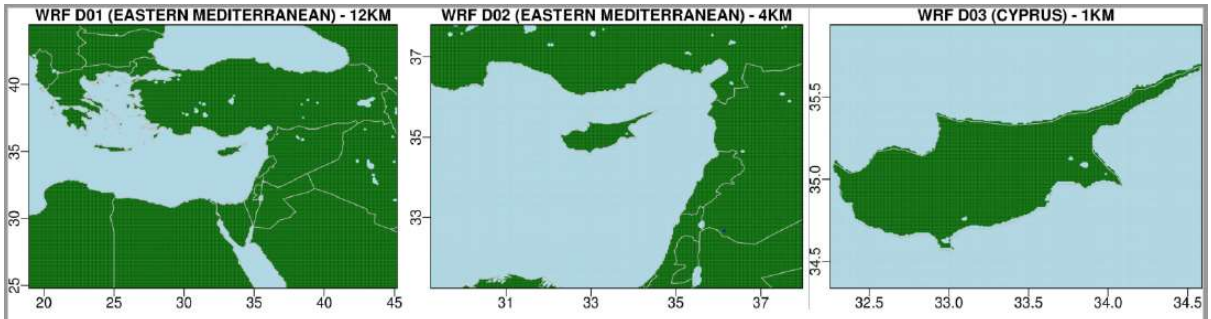

Figure. 1. Simulation domains of the eastern Mediterranean region centered over Cyprus for the 12 km (WRF-D01 – left panel), 4 km (WRF-D02 – middle panel) and 1 km (WRF-D03 – right panel) simulations.

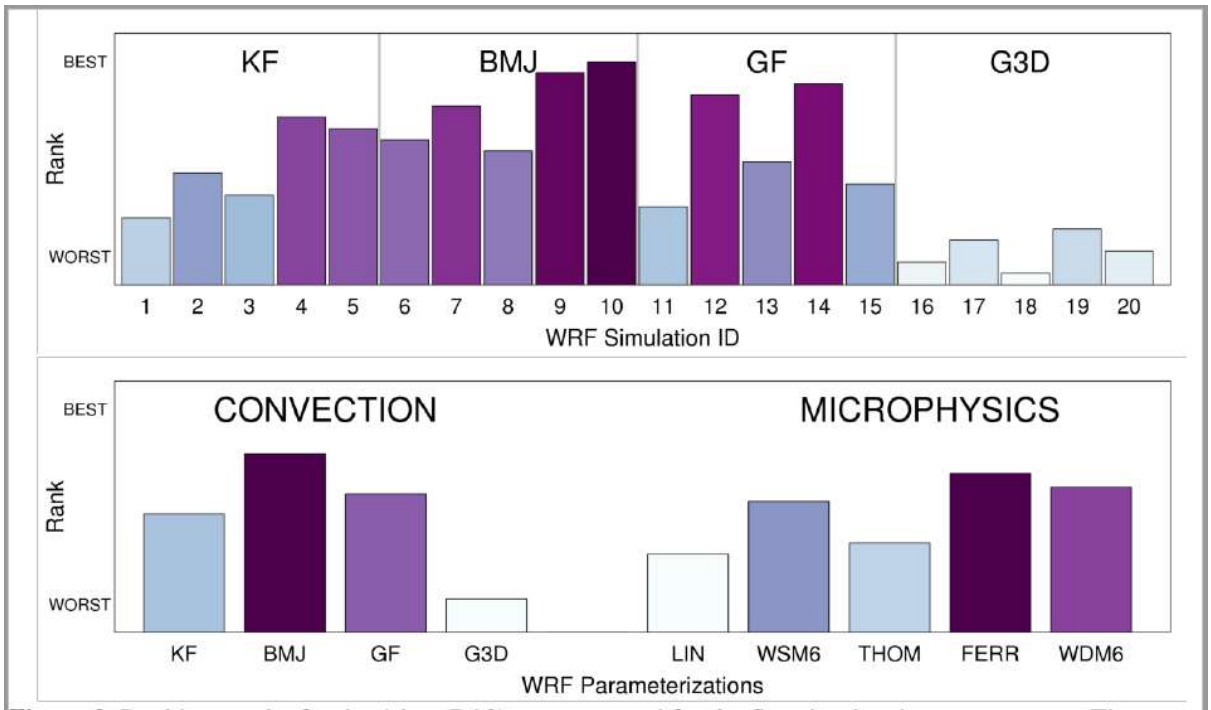

Figure 2. Ranking results for the 4-km (D02) nest averaged for the five simulated extreme events. The upper panel shows all 20 WRF configurations, while in the bottom panel simulations are grouped according to their convection and microphysics parameterizations. Darker colors indicate a higher ranking.

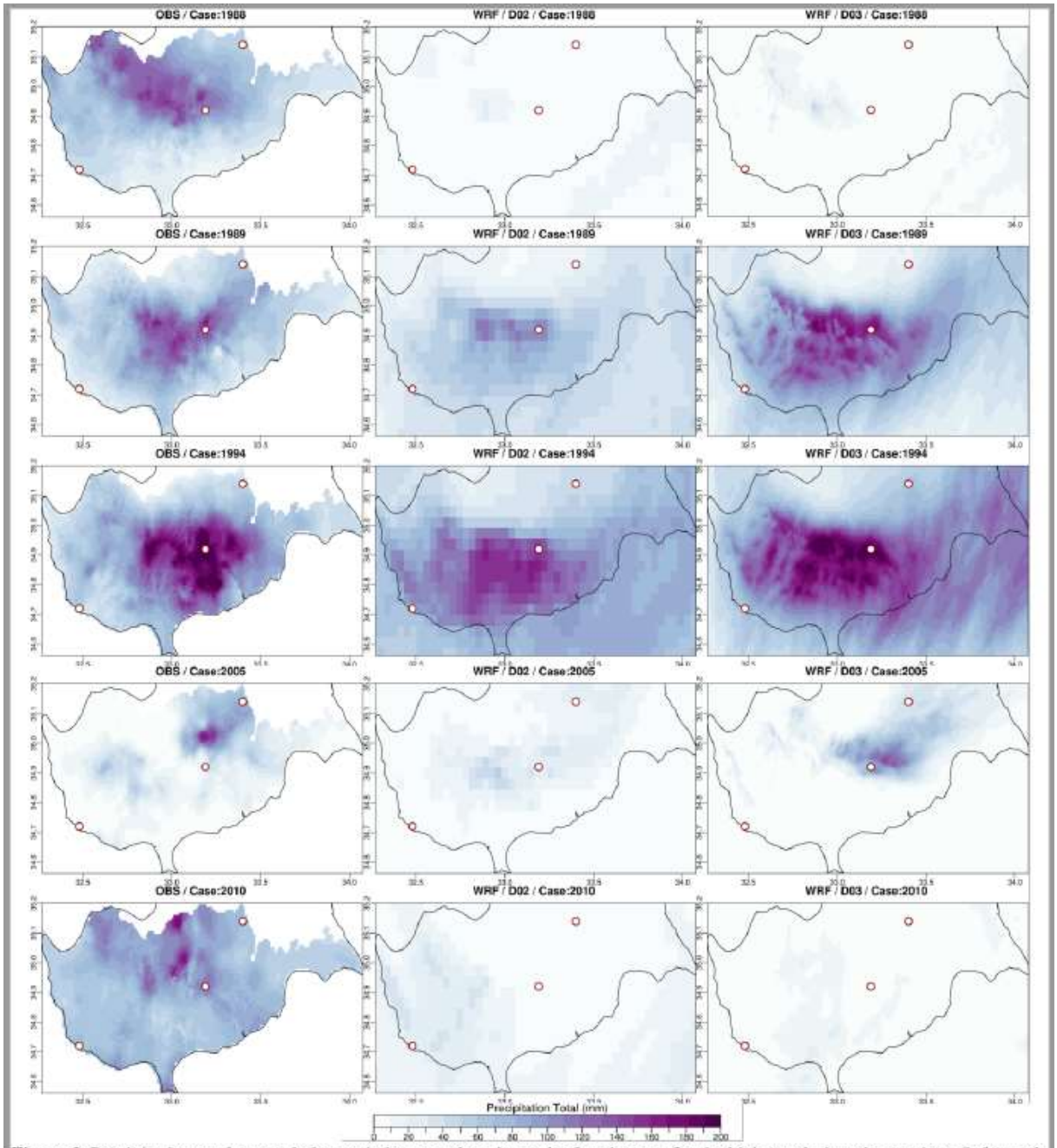

Figure 3. Precipitation total over a 3-day period centered on the peak of each event for the high-resolution observations (left panels the 4-km WRF-D02 (middle panels) and the 1-km WRF-D03 simulations (right panels). The latter represent the ensemble mean o the five best WRF simulations

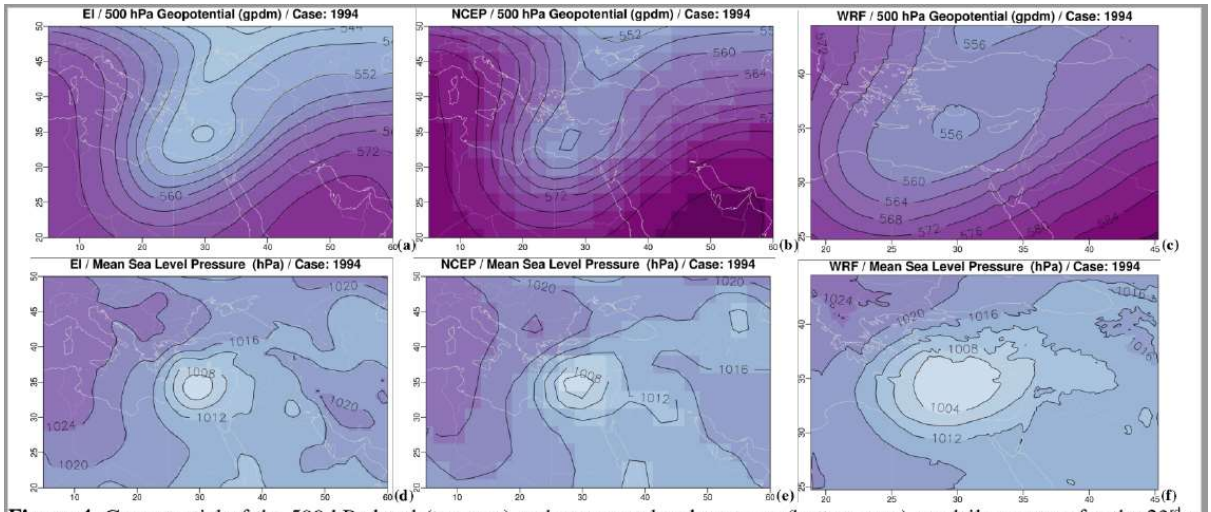

Figure 4. Geopotential of the 500 hPa level (top row) and mean sea level pressure (bottom row), as daily average for the 23rd o November 1994 and based on the ERA-Interim (left column), NCEP reanalysis (middle column) and WRF 12-km simulations (righ column).

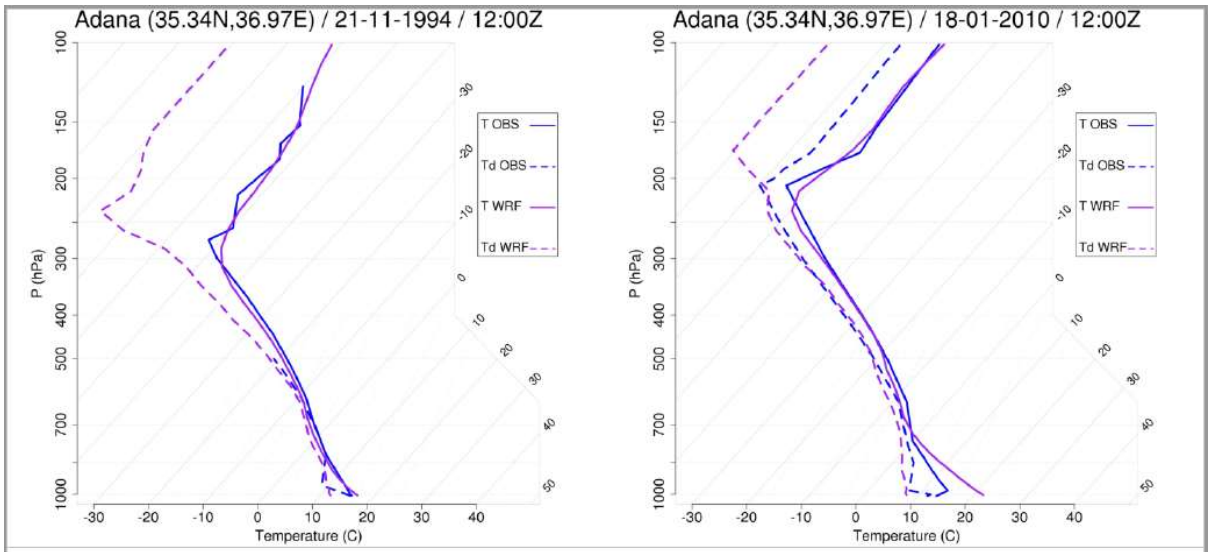

Figure 5. Vertical structure of the atmosphere for temperature (T) and dew point temperature (Td) based on observations (blue) and WRF 12-km simulations (purple) for the November 1994 (left panel) and the January 2010 (right panel) events. Radiosonde launched on Adana station in south Turkey.

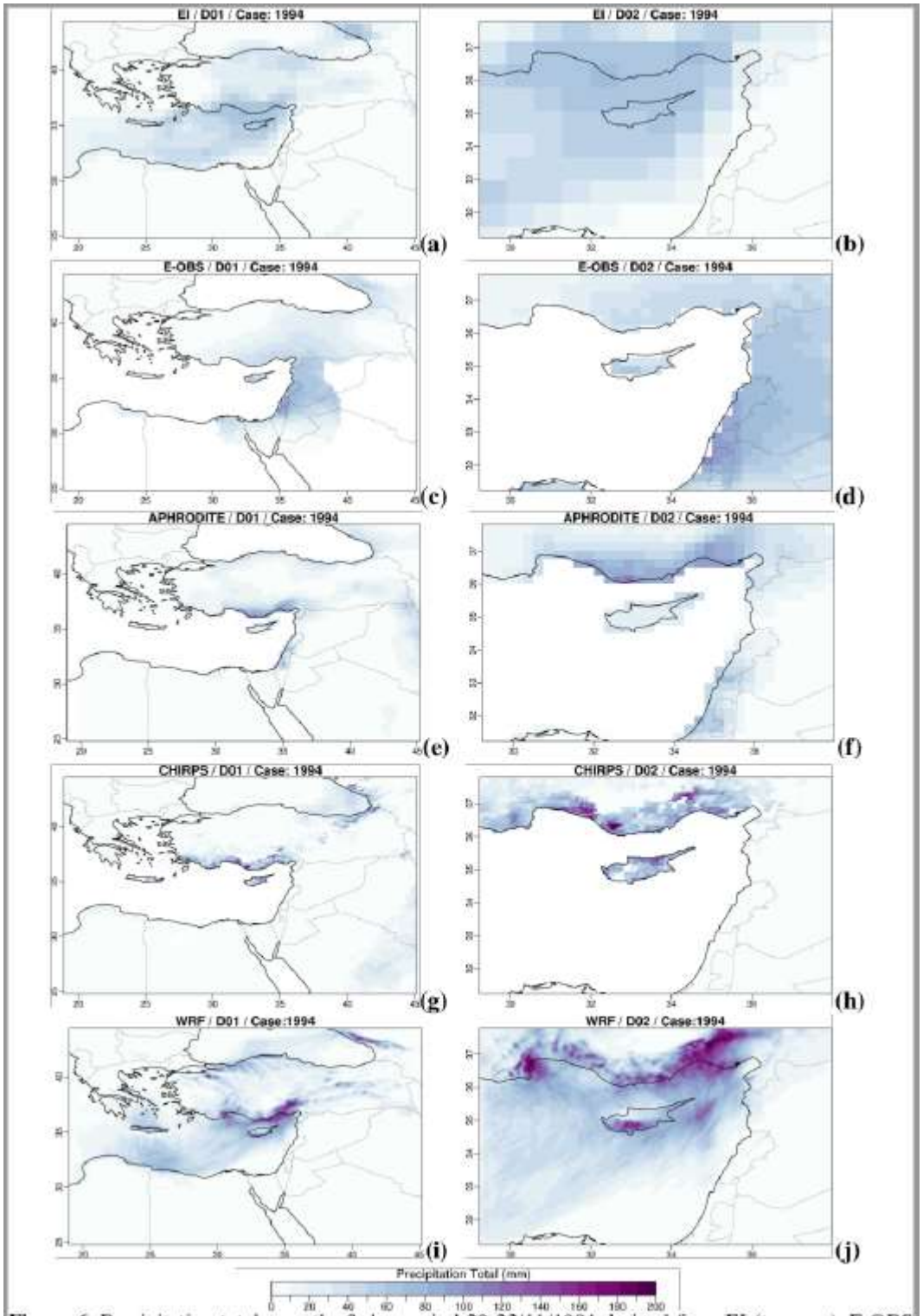

Figure 6. Precipitation total over the 3-day period 20-22/11/1994 derived from EI (top row), E-OBS (second row), APHRODITE (third row), CHIRPS (fourth row) and the ensemble mean of the five best WRF simulations (bottom row) for the 12-km (left panels) and 4-km (right panels) domains.

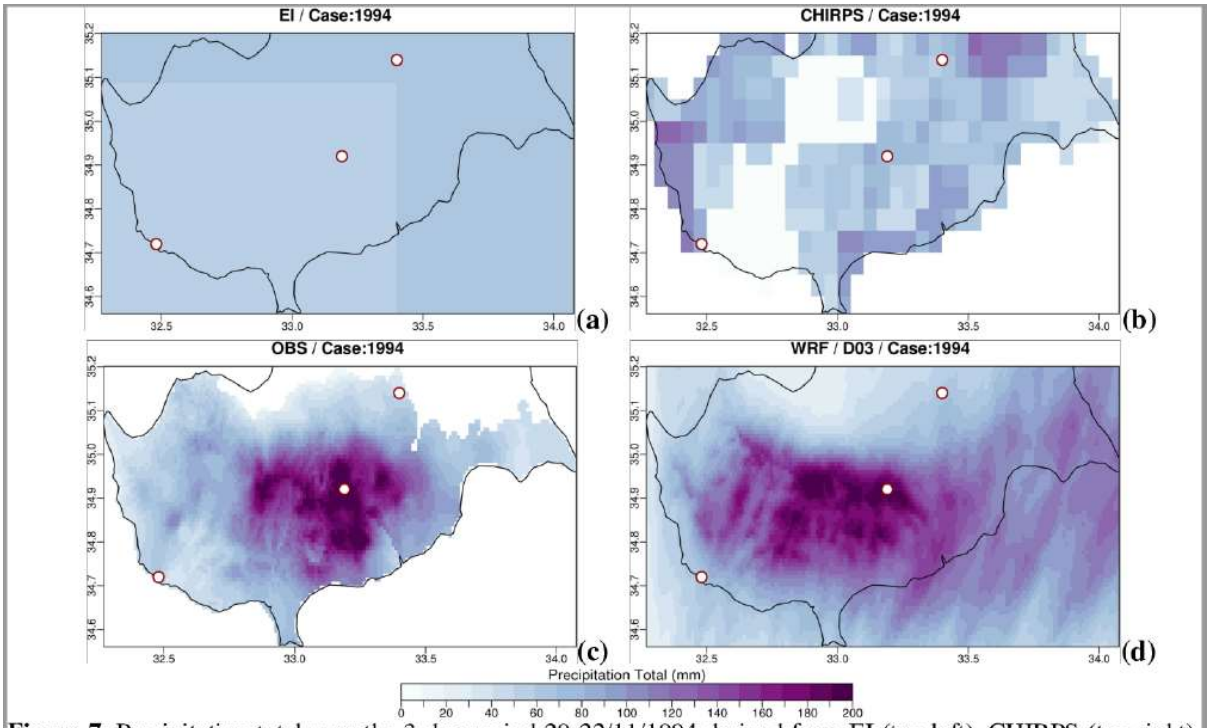

Figure 7. Precipitation total over the 3-day period 20-22/11/1994 derived from EI (top left), CHIRPS (top right), high-resolution Cyprus observations (bottom left), and ensemble mean of the five best WRF simulations (bottom right) for the 1-km domain. Points indicate the locations of the three weather stations for the time series comparison in Figure 8, from west to east: Pafos, Kionia, Nicosia.

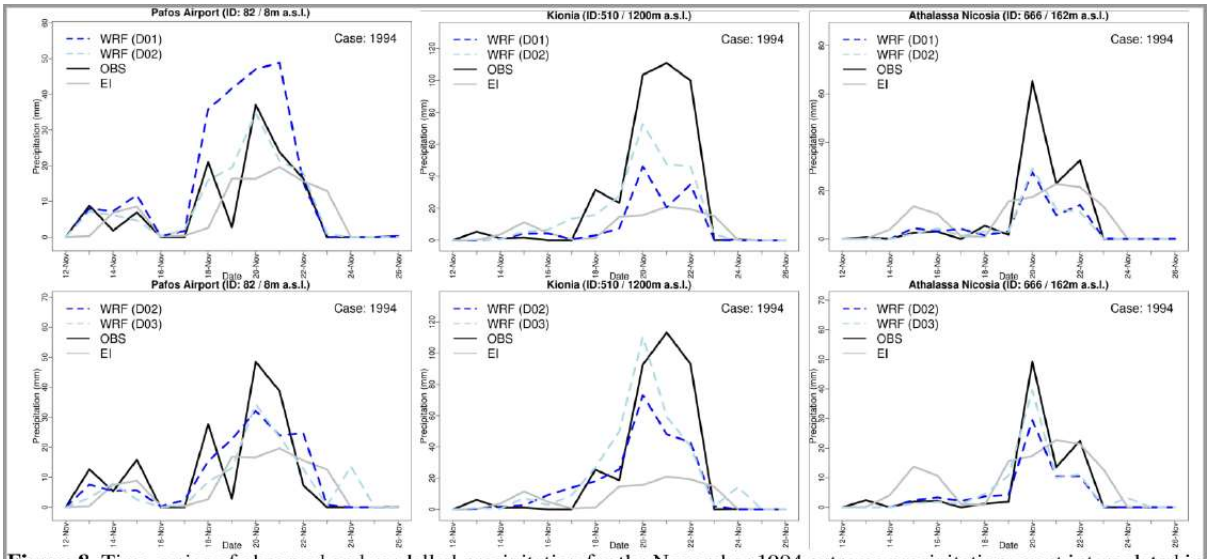

Figure 8. Time-series of observed and modelled precipitation for the November 1994 extreme precipitation event interpolated in the 12km (top row) and 4km (bottom row) grids for the stations of Pafos, Kionia and Athalassa.

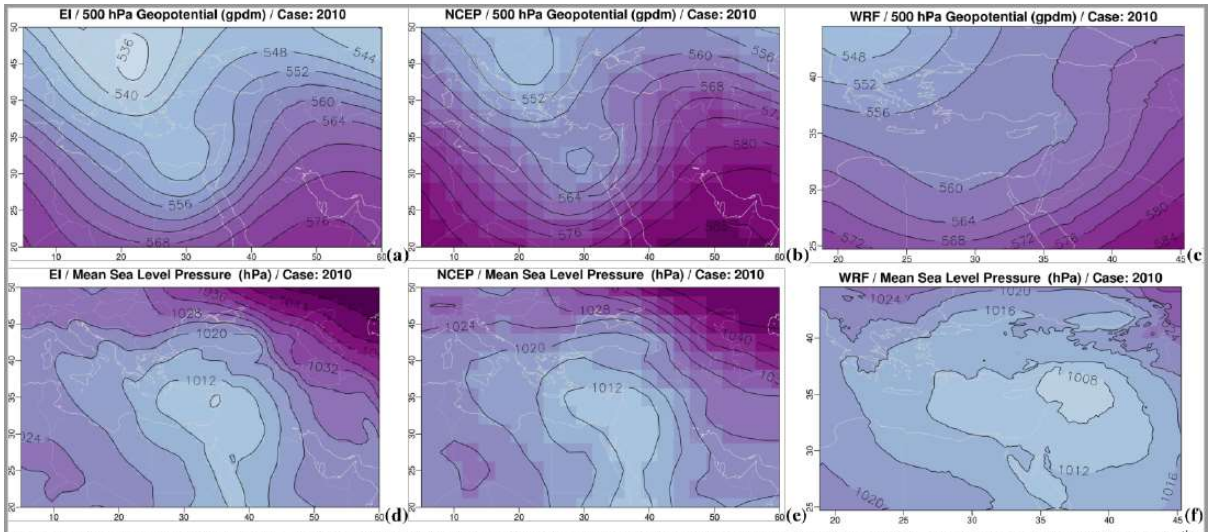

Figure 9. Geopotential of the 500 hPa level (top row) and mean sea level pressure (bottom row), as daily average for the 18th of January 2010 and based on the ERA-Interim (left column), NCEP reanalysis (middle column) and WRF 12-km simulations (right column).

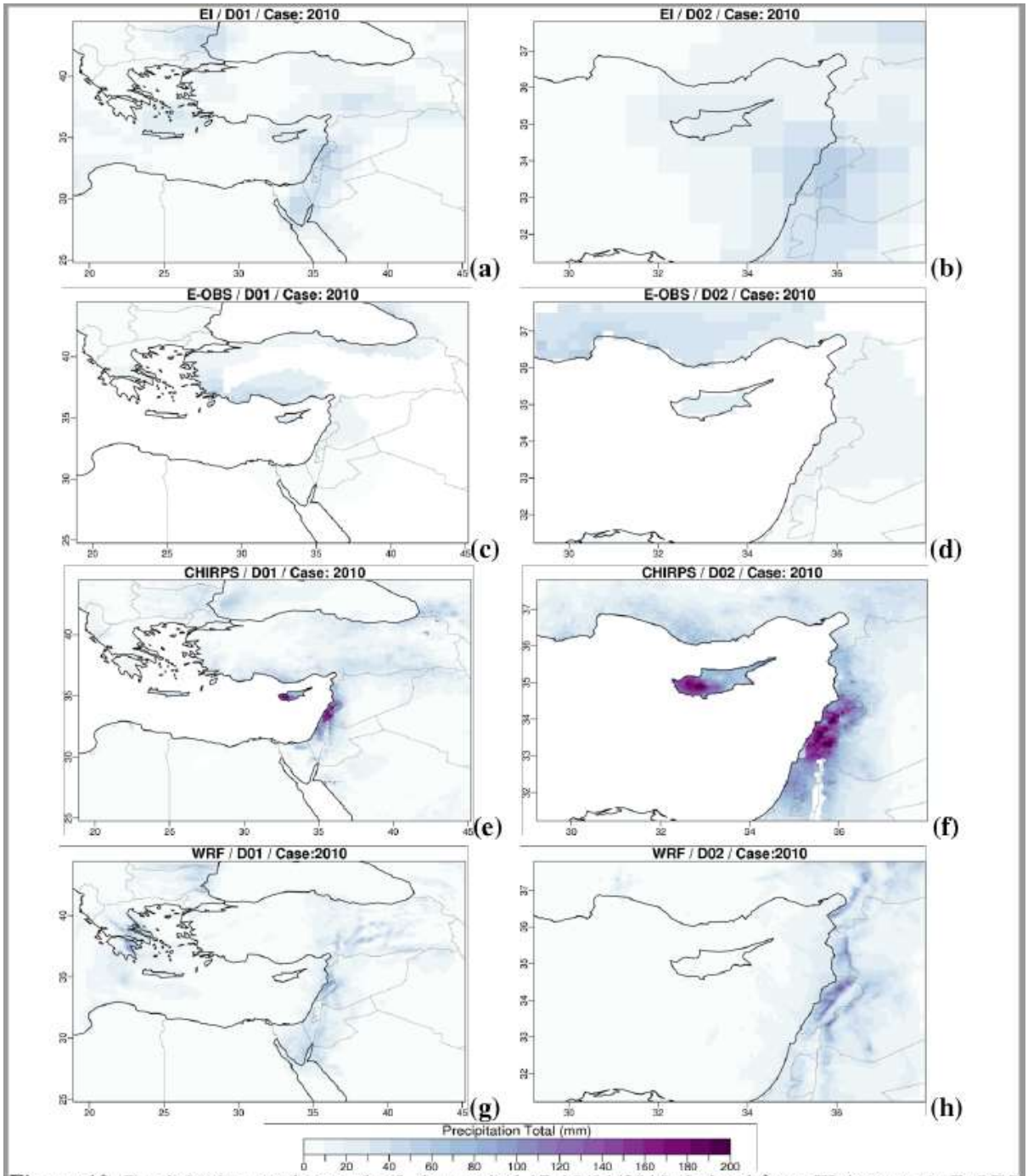

Figure 10. Precipitation total over the 3-day period 17-19/01/2010 derived from EI (top row), E-OBS (second row), CHIRPS (third row) and ensemble mean of the five best WRF simulations (bottom row) for the 12-km (left panels) and 4-km (right panels) domains.

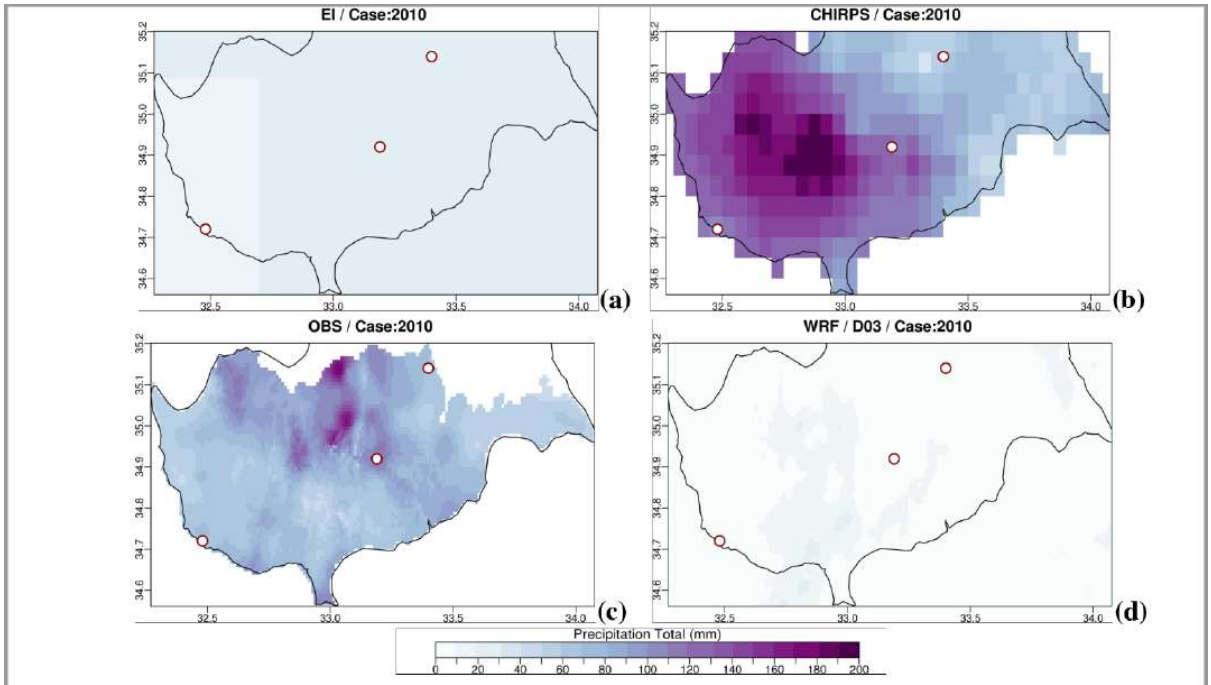

Figure 11. Precipitation total over the 3-day period 17-19/01/2010 derived from EI (a), CHIRPS (b), high-resolution Cyprus observations (c), and ensemble mean of the five best WRF simulations (d) for the 1-km domain. Points indicate the locations of the three weather stations for the time series comparison in Figure 12, from west to east: Pafos, Kionia, Nicosia.

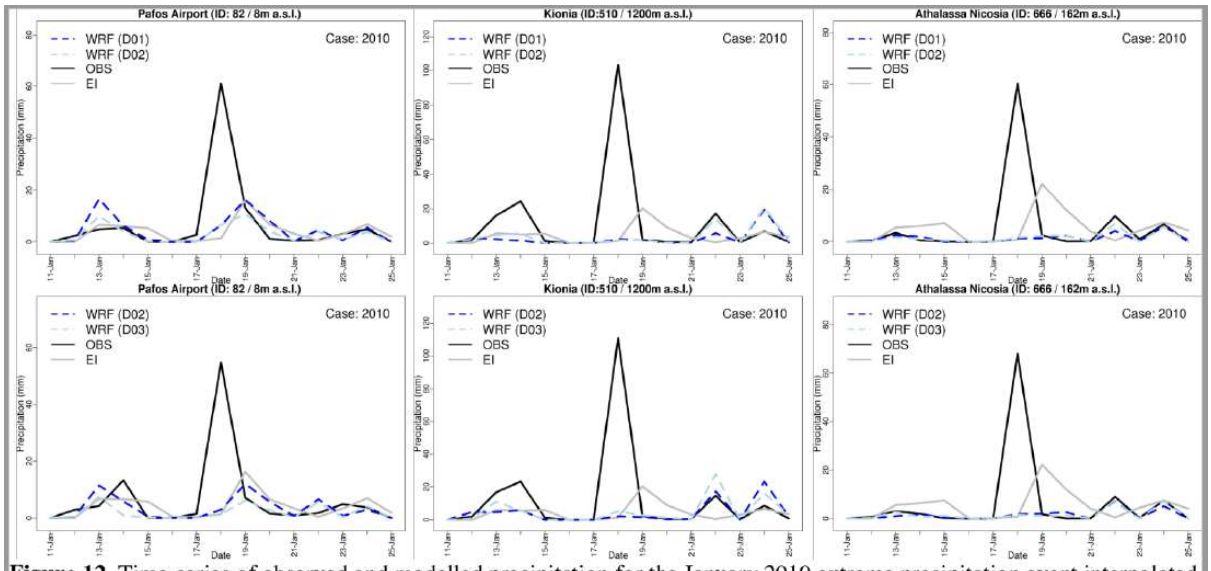

Figure 12. Time-series of observed and modelled precipitation for the January 2010 extreme precipitation event interpolated in the 12km (top row) and 4km (bottom row) grids for the stations of Pafos, Kionia and Athalassa.